AUTOMATED CROPPING AND ARTIFACT REMOVAL FOR KNIFE-EDGE SCANNING MICROSCOPY

Jaerock Kwon

Kettering University
Electrical & Computer Engineering
Flint, MI

David Mayerich

University of Illinois
Beckman Institute
Urbana-Champaign, IL

Yoonsuck Choe

Texas A&M University
Computer Science & Engineering
College Station, TX

ABSTRACT

Knife Edge Scanning Microscopy (KESM) is a high-throughput imaging technique used to obtain large-scale anatomical information ($\approx$ 1cm^3) at sub-micrometer resolution. Data acquisition has been fully automated, however significant post-processing and reconstruction must be done manually. KESM is unique in that illumination and tissue sectioning are performed using a diamond knife. Therefore many of the physical forces applied to the knife (e.g., vibration, slip, and light refraction) manifest as image artifacts and must be removed in post-processing. In this paper, we propose a fully automated framework to extract valid data from imaged sections and remove lighting artifacts, allowing reconstruction of the volumetric structures in multiple terabyte-scale data sets.

***Index Terms*—** Knife-edge Scanning Microscopy, KESM, serial sectioning microscopy, noise removal, cropping

1. INTRODUCTION

The Knife Edge Scanning Microscope (KESM) is a high-throughput instrument used for sectioning and imaging large tissue blocks at sub-micrometer resolution (Fig. 1) [1]. While previous work has shown that data throughput can be improved using automation [2], much of the required post-processing and reconstruction must be done manually. In data sets exceeding several terabytes per specimen, this process can be extremely time-consuming.

Two major post-processing steps are required to reconstruct a KESM volume. First, valid tissue data in raw KESM images must be located and extracted. Second, lighting artifacts inherent to the imaging process must be removed.

In this paper, we propose fully automated methods for region cropping and artifact removal. We use our methods to process two data sets ($\sim$ 2 TB each) representing the whole mouse brain at sub-micron resolution in all three dimensions.

This work was funded in part by NIH/NINDS grant #R01-NS54252 and NSF CRCNS #0905041. We would like to thank B. H. McCormick (KESM design), L. C. Abbott (tissue preparation), J. Keyser (graphics), and B. Mesa (KESM instrumentation).

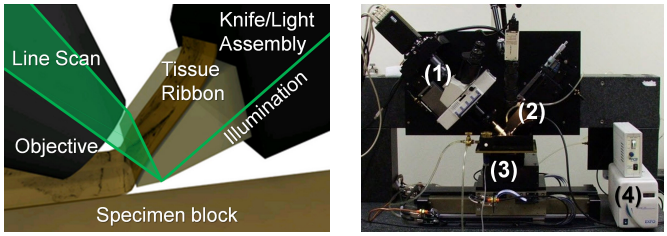

(a) (b)

Fig. 1. Knife-Edge Scanning Microscopy. (a) Specimen is undergoing sectioning by the KESM. Diamond knife collimator supports transmission illumination. (b) A full view of the KESM. (1) Microscope and camera assembly, (2) knife assembly, (3) the stage, and (4) white light illuminator.

By using the proposed methods, we show that volumetric data from KESM image stacks can be clearly examined and analyzed to obtain high-resolution structural detail for volume sizes that are very hard to obtain using standard microscopy.

2. AUTOMATIC CROPPING

KESM operates by simultaneously cutting and imaging blocks of tissue into sections that are typically 0.6 to 2 mm wide [2]. The raw sections are arranged into neighboring stacks ($\approx$ 9,000 in each stack) that must be assembled to create the final volume. Since it is virtually impossible to precisely align the optics such that a tissue section occupies the exact field-of-view of the objective, each image contains spurious data that must be properly removed. The images can then be aligned with their neighbors into a mosaic representing a cross-section of the data set.

2.1. Image Chunk Misalignment

By design, KESM does not require image registration since each section is imaged before significant deformation can occur. However, small perturbations in knife position can cause misalignment of images in a single stack. This occurs any

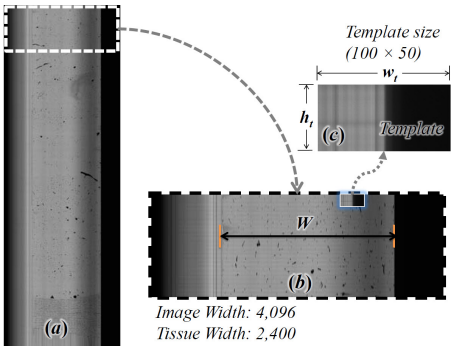

Fig. 2. Cropping by template matching. (a) An example of a captured image. (b) Part of an image shows the tissue width. (c) Sliding template (100 × 50).

time that the knife is moved due to misalignments between cutting sessions, power outage, maintenance, etc.

These misalignments can occur hundreds of times while imaging a single specimen, making cropping a time consuming manual job for data sets that can exceed several terabytes. We first describe an automated method for locating tissue regions in raw images using template matching based on the sum of the difference [3]:

$$d(x,y) = \sum_{c=0}^{(w_t-1)} \sum_{r=0}^{(h_t-1)} |p_s(x+c, y+r) - p_t(c,r)| \quad (1)$$

where w_t and h_t are the width and height of the template image respectively, p_s is a point in the raw image, and p_t is a point in the template image.

The left edge of the tissue is low-contrast and difficult to detect, however the right edge (at the knife corner) shows a clear difference between foreground (tissue) and background information. The start position of the template in the raw image is the minimum value of $d(x,y)$ (Eq. 2), where the smallest difference exists between the template and the image.

$$d_{\min} = \min_x(d(x,y)) \quad (2)$$

Thus, the x start position of the tissue area can be calculated by Eq. 3

$$x_{\text{start}} = \left(d_{\min} + \frac{w_t}{2}\right) - W \quad (3)$$

where W is the width of the region containing data.

3. KESM VOLUME NOISE

KESM exhibits several types of imaging artifacts that degrade or distort the acquired volumetric data. Many of the artifacts in KESM imaging are caused by lighting irregularities, primarily due to the use of the knife edge as a collimator/light source as well as a cutting device. These irregularities are caused by several factors, including the refraction of light through the knife (an imperfect lens) as well as physical defects (chips, nicks) in the knife edge and surface. In addition, uniform illumination across the knife edge would require perfect alignment of the optics, which is impossible at the tolerances required for high-throughput imaging. These errors cause uneven illumination in an image along the horizontal direction.

3.1. Irregular Lighting Artifacts

Possible sources of defects are as follows: (1) non-uniform illumination across the knife edge (caused by refraction and misalignment of the optics), creating intensity irregularities across the *width* of the image. (2) Fluctuation in illuminator power. (3) Different exposure time due to changing cutting velocity [4].

This final source of artifacts results from randomizing cutting velocity, which is used to reduce knife vibration artifact. This technique of changing velocity to suppress chatter has been addressed in the literature [4] and results in global intensity shifts from image to image.

The most widespread artifact in KESM imaging is caused by extreme lighting irregularities and knife chips. These artifacts result in a loss of information in the affected region.

3.2. Image Processing Techniques

We specifically focus on image processing techniques that use local information so that the processing can be run on heterogenous systems in parallel. Parallelism in data processing is important for dealing with large, multi-terabyte volumes. Local smoothing is often used to remove high-frequency noise [5]. However, KESM data sets have high-frequence and low-contrast images. So the smoothing technique cannot be used for KESM data. Our initial approach is to scale the pixel values in a line by the average of a small window of pixels surrounding the current pixel in the line. This method suffers from uneven equalization in and around excessively dark or bright areas. To address this problem, we use median intensity levels as baseline values, which eliminates artifacts introduced through processing (Fig. 3).

Our first step is to normalize overall intensity levels within an image. Each pixel in a row is normalized based on the median intensity value. The same process is applied for each column:

$$T_x = \frac{p(x,Y)}{\text{M}(\text{R}(I,Y))} \times L \quad (4)$$

$$T_y = \frac{p(X,y)}{\text{M}(\text{C}(I,X))} \times L \quad (5)$$

$$\bar{I} = \forall_x T_X \left(\forall_y T_Y (I,y), x\right) \quad (6)$$

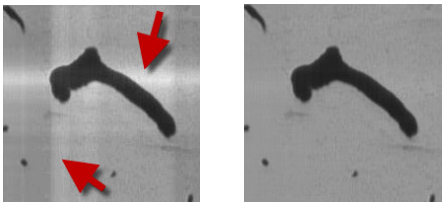

(a) (b)

Fig. 3. Comparison of the average value baseline method with the median value baseline one. The proposed method removes white artifacts around foreground objects. (a) Uneven equalization (see regions pointed by arrows) from the average value baseline method. (b) Evenly equalized intensity level from the proposed method.

where T_x is a normalized row , T_y is a normalized column, $p(x, y)$ is the pixel value at (x, y), $\mathrm{M}(\cdot)$ is the median value of a series of pixels, L is defined as a base line background intensity level to normalize the inter-image intensity difference, $\mathrm{R}(I, Y) = \forall_x p(x, Y)$, $\mathrm{C}(I, X) = \forall_y p(X, y)$, $I = \forall_x \forall_y p(x, y)$, and $\bar{I}$ is the normalized image. See Algorithm 1 for more details of the normalization process.

Algorithm 1 Normalization

$R_{max} \leftarrow$ MaxRowInImage
$C_{max} \leftarrow$ MaxColumnInImage
$L \leftarrow$ BaseLineBackgroundIntensityLevel
{Do normalize all columns}
while $y < C_{max}$ **do**
  while $x < R_{max}$ **do**
    $p(x, y) = p(x, y) \times L / \mathrm{M}(\mathrm{R}(I, y))$
{Do normalize all rows}
while $x < R_{max}$ **do**
  while $y < C_{max}$ **do**
    $p(x, y) = p(x, y) \times L / \mathrm{M}(\mathrm{C}(I, x))$

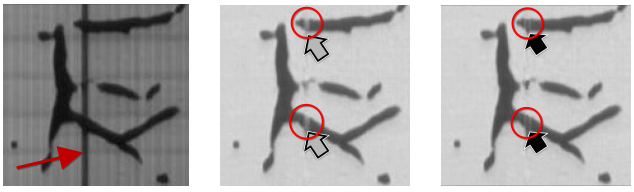

(a) (b) (c)

Fig. 4. Selective normalization. (a) An example of excessively dark vertical artifacts (arrow). (b) Foreground objects (arrows) become too bright. (c) Fixing over-normalization. Foreground objects (arrows) are properly recovered.

Noise from non-uniform illumination and knife defects are removed using intensity normalization. However, this is insufficient when the stripes are excessively dark and cause data loss. The excessiveness can be determined by the clear distinction between intensity levels of background and foreground objects. In other words, the dark stripes are *excessive* if the intensity levels of the background are nearly indistinguishable from those of the foreground objects. The intensity levels of foreground objects after normalization based on median values are even brighter than those of the background in the original image, meaning that normalized foreground objects become brighter than other foreground objects (see Fig. 4 (b)).

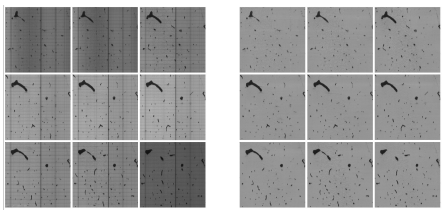

(a) (b)

Fig. 5. Normalization results of India-ink stained mouse brain vascular/microvascular system. (a) The original images before normalization. The images have dark vertical lines and uneven intensities across the horizontal direction. (b) Foreground information in vertical lines are restored and uneven intensity levels are successfully removed. Mouse brain with the vasculature stained with india ink is shown.

To address this, we introduce a *Selective Normalization* method which maintains the intensity levels of foreground objects while normalizing those of background objects if the current background value is excessively dark. The detailed algorithm is described in Algorithm 2. Table 1 shows the parameters of the Selective Normalization for both the India-ink stained vascular data set and the Golgi stained neural data.

Parameter	Value
L (baseline background intensity)	150
τ (minimum median intensity)	75
ω (foreground object factor)	0.8

Table 1. Parameters for Selective Normalization

The foreground object factor, ω determines the threshold intensity level foreground pixels in excessively dark stripes. The method can be used for tissue types by adjusting these parameters according to the characteristics of the images without changing the algorithm.

Fig. 4 illustrates the process of selective normalization. As shown in Fig. 4 (b), general intensity normalization methods cause over-normalization. Algorithm 2 shows details and Fig. 4 (c) manifests the effectiveness of Selective Normalization method.

Algorithm 2 Selective Normalization

$R_{max} \leftarrow \text{MaxRowInImage}$
$C_{max} \leftarrow \text{MaxColumnInImage}$
$L \leftarrow \text{BaseLineBackgroundIntensityLevel}$
$\tau \leftarrow \text{MinMedianIntensity}$
$\omega \leftarrow \text{ForegroundObjectFactor}$
{Do normalize all columns}
while $y < C_{max}$ **do**
  while $x < R_{max}$ **do**
    if $M(\text{R}(I, y)) < \tau$ **then**
      if $p(x, y) < (M(\text{R}(I, y) \times \omega)$ **then**
        {pixel belongs to foreground}
        $p(x, y) = p(x, y)$
      else
        {pixel belongs to background}
        $p(x, y) = p(x, y) \times L/M(\text{R}(I, y))$
{Do normalize all rows}
while $x < R_{max}$ **do**
  while $y < C_{max}$ **do**
    if $M(\text{C}(I, x)) < \tau$ **then**
      if $p(x, y) < (M(\text{C}(I, x) \times \omega)$ **then**
        {pixel belongs to foreground}
        $p(x, y) = p(x, y)$
      else
        {pixel belongs to background}
        $p(x, y) = p(x, y) \times L/M(\text{C}(I, x))$

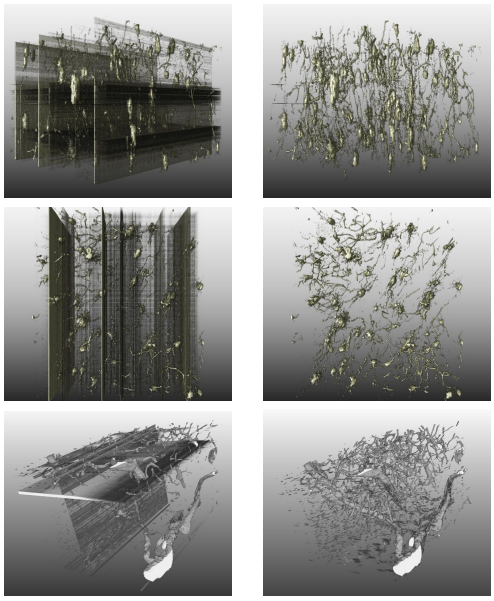

(a) (b)

Fig. 6. Qualitative comparison in Golgi-stained tissue showing neuronal distribution. Same image volumes are used in each row to compare their image quality. (a) Original volumes before normalization have many artifacts that prevent from being analyzed properly. (b) Processed volumes show clear inner structures.

4. RESULTS

We processed two mouse brain three-dimensional images ($\sim$ 4 TB total) using the fully automated methods for region cropping and artifact removal. Fig. 4 shows that *Selective Normalization* method can fix the over-normalization problem. Fig. 5 shows that our proposed methods can efficiently remove vertical artifacts and uneven inter-image intensity levels. Qualitative comparision in Fig. 6 demonstrates the effectiveness of the proposed methods. The results show that the processed volumes reveal clear internal connectivity structures.

5. CONCLUSION

Unprecedented amounts of high-resolution images prevent us from removing artifacts manually or semi-automatically. We provide a fully automated framework for extracting regions that contain tissue data, correcting stack alignment, and correcting artifacts resulting from non-uniform intensity and knife defects. Our approach allows us to turn the KESM data into a valuable resource for neuroscientists.

6. REFERENCES

[1] David Mayerich, Louise C. Abbott, and Bruce H. McCormick, "Knife-edge scanning microscopy for imaging and reconstruction of three-dimensional anatomical structures of the mouse brain," *Microscopy*, vol. 231, pp. 134–143, July 2008.

[2] Jaerock Kwon, David Mayerich, Yoonsuck Choe, and Bruce H. McCormick, "Automated lateral sectioning for Knife-Edge scanning microscopy," in *Biomedical Imaging: From Nano to Macro, 2008. ISBI 2008. 5th IEEE International Symposium on*, 2008, pp. 1371–1374.

[3] Trung Tran, Hyo-Moon Cho, and Sang-Bock Cho, "Performance enhancement of sum of absolute difference (SAD) computation in H.264/AVC using saturation arithmetic," in *Emerging Intelligent Computing Technology and Applications*, pp. 396–404. 2009.

[4] Marian Wiercigroch and Erhan Budak, "Sources of nonlinearities, chatter generation and suppression in metal cutting," in *Philosophical Transactions of the Royal Society*, 2001, vol. 359, pp. 663–693.

[5] Darwin T. Kuan, Alexander A. Sawchuk, Timothy C. Strand, and Pierre Chavel, "Adaptive noise smoothing filter for images with signal-dependent noise," in *IEEE Transactions on Pattern Analysis and Machine Intelligence*, 1985, vol. 7, pp. 165 – 177.